PERGAMON

International Journal of Heat and Mass Transfer 41 (1998) 3857–3871

International Journal of HEAT and MASS TRANSFER

An experimental investigation of bubble growth and detachment in vertical upflow and downflow boiling

G. E. Thorncroft[a], J. F. Klausner[a,*], R. Mei[b]

[a] *Department of Mechanical Engineering*, [b] *Department of Aerospace Engineering, Mechanics and Engineering Science, University of Florida, Gainesville, FL 32611, U.S.A.*

Received 17 March 1997; in final form 23 February 1998

Abstract

A visual study of vapor bubble growth and departure in vertical upflow and downflow forced convection boiling is presented. A vertical flow boiling facility was constructed with a transparent, electrically-heated test section in which the ebullition process could be observed. High-speed digital images of flow boiling phenomena were obtained, which were used to measure bubble growth, departure diameters, and lift-off diameters. Experiments were conducted for flow of FC-87 over a commercially-finished nichrome heating surface, with mass flux ranging from 190 to 666 kg m^{-2} s^{-1} and heat flux ranging from 1.3 to 14.6 kW/m^2. The flow was slightly subcooled (ΔT_{sub} = 1.0–5.0°C), and boiling occurred at isolated nucleation sites. A major conclusion of this work is that the observed vapor bubble dynamics between upflow and downflow are significantly different. In the upflow configuration, bubbles departing the nucleation site slide along the heater wall, and typically do not lift off. In the downflow configuration, bubbles either lift off directly from the nucleation site or slide and then lift off, depending on flow and thermal conditions. The process of vapor bubble sliding appears to be responsible for enhanced energy transfer from the heating surface, as evidenced by larger heat transfer coefficients for upflow than for downflow under otherwise identical operating conditions.

Key words: Boiling; Heat transfer; Vapor bubble dynamics

Nomenclature

C_p specific heat [J kg^{-1} K^{-1}]
$d(t)$ vapor bubble diameter [m or mm]
d_d vapor bubble departure diameter
d_L vapor bubble lift-off diameter
G liquid mass flux [kg m^{-2} s^{-1}]
h convective heat transfer coefficient [W m^{-2} K^{-1}]
h_{fg} latent heat of vaporization [J kg^{-1}]
Ja Jacob number, $\rho_l C_{pl} \Delta T_{sat}/\rho_v h_{fg}$
K mean growth constant [m s^{-n}]
n mean growth exponent
t time [s or ms]
t_w waiting time [ms]
T temperature [°C]
ΔT_b bulk fluid temperature difference, $T_w - T_b$ [°C]
ΔT_{sat} wall superheat, $T_w - T_{sat}$ [°C]
ΔT_{sub} bulk fluid subcooling, $T_{sat} - T_b$ [°C]
u_l mean liquid velocity [m s^{-1}]
u^* friction velocity [m s^{-1}]
q_w wall heat flux [kW m^{-2}]

Greek symbols

λ^+ dimensionless integral length scale
λ integral time scale [m]
v kinematic viscosity [m^2 s^{-1}]
ρ density [kg m^{-3}]
τ integral time scale [s]

Subscripts

b bulk liquid
l liquid

* Corresponding author. Tel.: 007 352 392 3506; fax: 007 352 392 1071; e-mail: klaus@nersp.nerdc.ufl.edu

0017–9310/98 $19.00
PII: S0017–9310(98)00092–1

sat saturation
sub subcooling
w wall (heater surface)
v vapor

1. Introduction

The high heat transfer rates associated with forced convection boiling are due to two complex processes working together: bulk turbulent convection, and the growth and detachment of vapor bubbles at the heating surface. In order to develop reliable predictions for forced convection boiling heat transfer, it is necessary to understand the complex thermal and hydrodynamic interaction between the liquid and vapor phases. However, limited experimental data is available in the literature for vapor bubble growth and detachment in flow boiling.

Studies which have sought to visually examine the vapor bubble growth and detachment processes in vertical flow boiling have focused largely on the upward flow configuration. Gunther [4] used high-speed cinematography to examine vapor bubble dynamics in subcooled, upflow boiling of water. Vapor bubble radii were measured during the growth and collapse stages in subcooled flow, and the effects of flow velocity and subcooling were documented. Hsu and Graham [6] performed a similar visual study with highly subcooled water to investigate the hydrodynamic features of bubbly and slug flow regimes in vertical upflow boiling, although no measurements of bubble growth rate or departure diameter were made. Jiji and Clark [7] photographed nucleation and measured flow temperature profiles for vertical upflow boiling of water under varying pressure. Frost and Kippenhan [3] measured growth rates and departure diameters of bubbles in subcooled upflow of water containing various concentrations of a surface active agent. Cooper et al. [1] measured bubble growth and displacement in supersaturated *n*-hexane in forced laminar upflow over a stationary wall. Similar measurements were made for short duration microgravity flow. Recently, van Helden et al. [17] obtained bubble growth, departure diameter, and trajectory data from artificial cavities during upflow of saturated and superheated water. In a follow-up study, van der Geld et al. [18] demonstrated that the angle at which the vapor bubbles lift off from the heater surface depends on the bulk liquid velocity as well as the surface temperature.

Several studies of vapor bubble dynamics have focused on horizontal flow boiling. Koumoutsos et al. [12] measured vapor bubble lift-off radii from an artificial nucleation site with saturated water flowing horizontally. Klausner et al. [11] measured departure and lift-off diameters for stratified two-phase horizontal flow boiling of R113. More recently, Kandlikar et al. [8] examined the effect of flow rate, subcooling, and wall superheat on the nucleation behavior of surface cavities in subcooled horizontal flow boiling of water. In a related study, Kandlikar et al. [9] examined the effect of flow velocity, wall superheat, and subcooling on the vapor bubble growth rate, and compared growth rates in flow boiling to those for pool boiling.

Attempts to model the vapor bubble dynamics in flow boiling have had limited success, due in large part to a lack of available experimental data. A recent model was developed by Klausner et al. [11] to predict departure and lift-off diameters for horizontal flow boiling, and extended by Zeng et al. [21] to include pool boiling. The model agrees well with a wide range of departure and lift-off diameter data reported in the literature. However, a satisfactory model for vertical flow boiling is not available, and Zeng et al. [21] express uncertainty concerning a general extension of their model to vertical flow boiling, for the following reasons. In the vertical upflow configuration, their model qualitatively predicts that a shear force pushes the rising bubble against the heating surface to prevent lift-off from the surface. Whether a mechanism exists to remove vapor bubbles from the heating surface remains uncertain. For the vertical downflow configuration, bubbles lag the liquid velocity, resulting in an outward-directed shear force which should be sufficient to lift vapor bubbles off the heating surface.

The existing vertical flow boiling bubble dynamic data are limited, and to the best of the authors' knowledge, no downflow boiling vapor bubble dynamic data have been reported. The purpose of this work is therefore to experimentally investigate the vapor growth and removal processes in vertical upflow and downflow boiling. An experimental facility using FC-87 as a working fluid has been designed, tested, and calibrated which allows visual examination of the ebullition process under slightly (1.0–5.0°C) subcooled conditions. High-speed digital video images of the flow are analyzed to obtain vapor bubble growth, departure diameter, lift-off diameter, and waiting time during vertical flow boiling from isolated nucleation sites.

2. Experiment description

2.1. *Experimental facility*

A schematic diagram of the experimental facility used in this work is shown in Fig. 1. A variable speed gear pump drives the working fluid through the facility. The volumetric flow rate is measured using either a venturi- or vane-type flow meter, each used to measure a different range of flow rates (venturi, 0.0–1.8 l min^{-1}; vane, 3.0–9.0 l min^{-1}). Both meters are accurate to within $\pm 0.5\%$ of their respective full scale. The fluid is preheated via four 1 kW coil heaters, then directed through a series of valves to achieve vertical upflow or downflow in the test

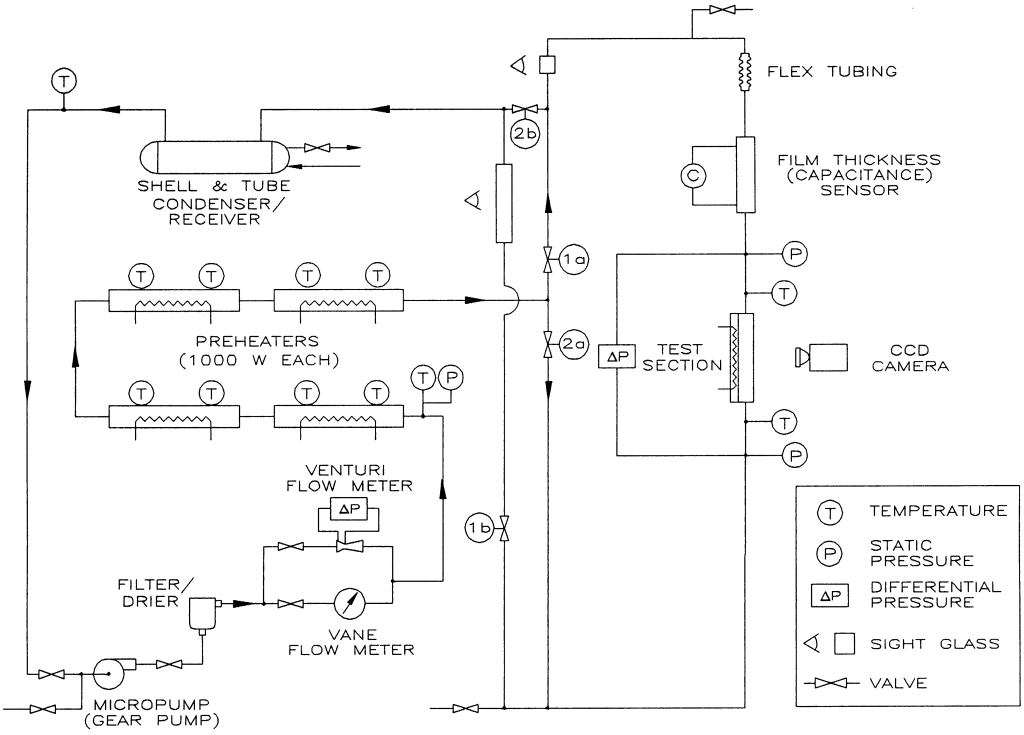

Fig. 1. Schematic diagram of vertical flow boiling facility.

section. The square test section uses a DC-powered nichrome heating strip, on which the average wall temperature and heat flux are measured. After exiting the test section the fluid enters a water cooled, shell-and-tube condenser/receiver which returns the fluid to a subcooled state. FC-87, a dielectric perfluorocarbon fluid, was selected as the working fluid for its low latent heat and moderate saturation temperature; a list of representative properties is given in Table 1. Measurements of pressure, temperature, and flow rate are recorded by a multiplexed 12-bit analog-to-digital converter attached to a personal computer. Since two-phase flows are inherently unsteady, 500 samples per channel are obtained over a period of 5 s and averaged to achieve repeatable measurements.

Table 1
Properties of saturated FC-87 at 1 ATM

Saturation temperature	29.3°C
Liquid density	1750 kg m^{-3}
Vapor density	12.5 kg m^{-3}
Enthalpy of vaporization	31.3 kJ kg^{-1}
Surface tension	8.97×10^{-3} N m^{-1}
Liquid dynamic viscosity	458×10^{-6} kg m^{-1} s^{-1}
Liquid specific heat	1.09 kJ kg^{-1} K^{-1}
Liquid Prandtl number	9.03

The transparent test section is illustrated in Fig. 2. The walls of the test section are constructed of 1/2 inch-thick, transparent, cast Lexan plate, bonded together with methacrylate resin to form a 12.7 mm ID square duct. A 30 cm long, 12.7 mm wide, 0.15 mm thick nichrome strip, clamped and adhered to one wall, is used as a heating surface. Six equally-spaced type-E thermocouples are attached to the underside of the nichrome strip to measure the average heater surface temperature. The thermocouples have an accuracy of ± 0.5°C. A one-dimensional, steady-state heat conduction analysis shows that the temperature difference between the underside of the heater and the side exposed to the flow is less than 0.05°C for the highest heat flux encountered in this study. This is well within the accuracy of the thermocouple itself. The test section is connected to the rest of the facility by flanges employing double O-ring face seals.

Electric power to the test section heater is supplied by a 0–50 V, 120 A DC rectifier. A digital voltmeter records the voltage across the heater with an uncertainty of ± 0.04 V. The electric current through the heater is determined by measuring the voltage drop across a 1 Ω shunt connected in series with the heater, with an uncertainty of ± 0.09 A. The maximum uncertainty in heat flux is approximately $\pm 1\%$. Heat losses through the test section were calibrated by measuring the difference between heater surface and ambient temperatures at various heat

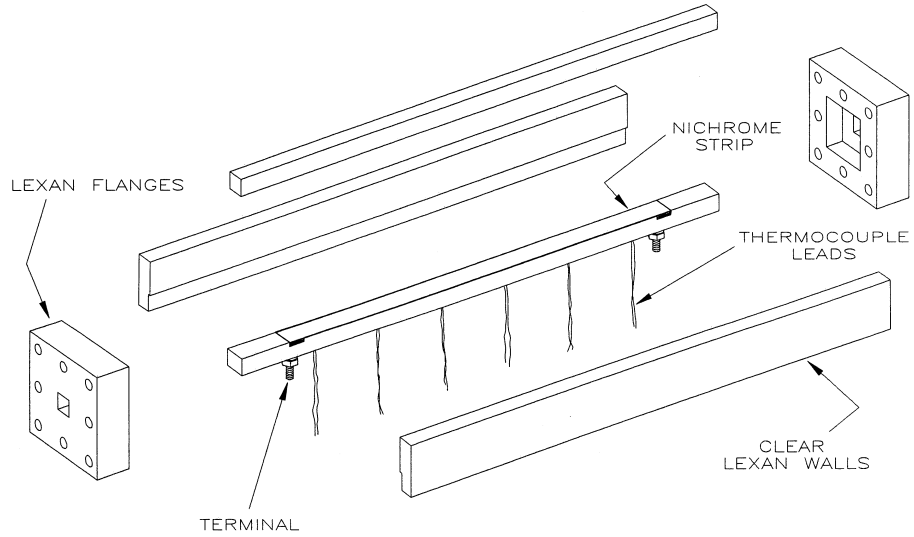

Fig. 2. Exploded view of visual test section.

fluxes during static tests with the system drained of working fluid. Two Viatran model 2416 static pressure transducers are installed immediately before and after the test section, both accurate to within ± 400 Pa. Two type-E thermocouples are also installed before and after the test section, and are used to measure bulk flow temperature. The bulk temperature difference, $\Delta T_b = T_w - T_b$, results from measurements of 6 wall thermocouples and 2 bulk flow thermocouples manufactured from the same roll, and is estimated to be accurate to within ± 0.5°C. The wall superheat, $\Delta T_{sat} = T_w - T_{sat}(P_{sat})$, and the subcooling, $\Delta T_{sub} = T_{sat}(P_{sat}) - T_b$, are based partly on the saturation temperature, which is calculated based on the measured static pressure at the test section inlet; both ΔT_{sat} and ΔT_{sub} are estimated to be accurate to within ± 0.6°C. It is further noted that additional uncertainty in the measurement of wall temperature is due to spatial variations in temperature which arise during nucleate boiling; this is discussed in detail in Section 2.2.

A Kodak EktaPro digital high-speed motion camera is used to obtain images of the ebullition process. Images with a resolution of 192×239 pixels are typically recorded at a rate of 2000 frames per s. The camera is equipped with a Vivitar 50 mm macro lens, resulting in an image field of approximately 2×4 mm (half-frame images) with a 20 μm resolution. A typical synchronous recording is comprised of 1600 images covering 800 ms in real time. An EktaPro EM Motion Analyzer stores the images which are then downloaded to a standard S-VHS video cassette recorder.

2.2. *Data collection and image analysis procedure*

The bulk single-phase conditions at the entrance of the test section are controlled by adjusting the preheat and flow rate. Once steady flow is established, power is applied to the test section heater at a sufficient rate to obtain vigorous boiling at the surface. The heat flux is then reduced until only isolated nucleation sites are active. Operating the facility in this matter eliminates the effect of boiling hysteresis.

The camera is mounted on a tripod, and is aimed at the heater from the side at approximately a 25–30° angle above the heater. In order to achieve the highest possible resolution and eliminate errors in calibration, the camera lens is fixed at a constant focal length, resulting in a fixed viewing area of approximately 4×4 mm (full-frame). Prior to filming, image calibration was performed by filming a scale in a separate but identical test section, at approximately the same angle to the test section. Image analysis is performed manually by measuring distances on the film as it is played back from video tape on a 20-in video monitor with 1000 lines per in resolution. The lateral displacement of the vapor bubble is the distance measured from the nucleation site to the bubble centroid. Bubble diameters were estimated as the chord length, measured through the bubble centroid, parallel to the heater surface. Since the camera was maintained normal to the direction of the flow, the error in measuring the bubble diameter due to optical distortion is minimized. Moreover, throughout this work the bubbles are very nearly spherical during the early portion of growth and sliding when the diameter is measured, so the bubble diameter as it is measured is judged to be an adequate representation of the bubble size.

An important consideration in these experiments involves the temporal and spatial variations in the heater surface temperature and the near-wall liquid velocity. Specifically, it is necessary to estimate the time scale of these variations to ensure that the film length is sufficient

to establish statistically meaningful values of mean bubble growth, departure and lift-off diameter, and sliding trajectory. For surface temperature, variations due to ebullition can be estimated using the time taken for growth and departure plus the waiting time. For experimental conditions examined in this work, this time scale is typically on the order of 20–50 ms. Velocity fluctuations may be estimated as follows. From a numerical simulation of single-phase turbulent channel flow [13], the integral length scale in the streamwise direction is on the order of $\lambda^+ = \lambda u^*/\nu_l \sim 500$. Thus an estimate of the time scale, assuming the frozen field hypothesis is valid, is on the order of $\tau = (500\ \nu_l/u^*)/u_l \sim 10^{-2}$–$10^{-1}$ s, where u_l is the mean liquid velocity in the duct, ranging from 0.10 to 0.19 m s^{-1} in this study. Considering both of these estimated time scales, the 800 ms film length is judged to be sufficient to capture the statistical variations in the measured bubble growth, departure and lift-off diameter, and trajectory. To ensure consistency of the film data, two to three films are captured at each condition.

3. Flow visualization

Table 2 summarizes the experimental conditions and data collected for vertical upflow and downflow boiling considered in this work. Twenty experimental conditions were studied, with mass fluxes ranging from 193 to 666 kg m^{-2} s^{-1} and heat fluxes ranging from 1.3 to 14.6 kW m^{-2}. The bulk flow was slightly subcooled, with ΔT_{sub} ranging from 1.0 to 5.0°C. One vertical surface pool boiling condition was also studied, which is included in the table as Exp. no. 8. All conditions examined in this work are within the nucleate boiling regime for which isolated nucleation sites are active.

3.1. *Upflow*

Figure 3(a) depicts a photograph of a stream of vapor bubbles originating from a single nucleation site in upflow, for $G = 258$ kg m^{-2} s^{-1}, $\Delta T_{sat} = 3.15$°C (Exp. no. 2b). The behavior shown is typical of upflow nucleation at low heat flux. At the nucleation site, the bubbles experience a short period of stationary growth, and then depart from the site by sliding upward. The bubbles accelerate to a greater velocity than that of the surrounding bulk flow. Measurement of bubble trajectories reveal that the bubble velocity exceeds the bulk velocity within 4 mm of the nucleation site, even for $G = 319$ kg m^{-2} s^{-1}, the largest mass flux considered in this work for upflow. Growth and departure is very regular, and the bubbles appear to be spherical in shape. The bubbles appear to remain attached to the heating surface and continue to grow while sliding along the surface. It is noted, however, that thermal gradients in the boundary layer and reflection of the bubble image on the heater surface make the location of the base of the bubble difficult to distinguish precisely. Figures 3(b) and 3(c) depict two other streams of bubbles originating from the same nucleation site. The field of view is approximately 10 mm and 30 mm downstream of the site, respectively. As the bubbles become larger, they become distorted, assuming a cap-like shape characteristic of bubbles rising faster than the surrounding flow. Bubbles are observed to oscillate laterally along the surface due to vortex shedding, but generally remain attached to the heating surface. Bubbles that lift off the surface do so randomly, and nonetheless tend to remain close to the heating surface.

The fact that the bubbles do not typically lift off the surface is qualitatively consistent with the supposition of Zeng et al. [21] that in upflow boiling, the sliding bubble leads the surrounding flow, and the resulting shear lift force pushes the bubble against the wall, preventing lift-off. Moreover, Gunther [4], Frost and Kippenhan [3], and Cooper et al. [1] report that bubbles remain attached to the heater surface during upflow following departure from the nucleation site. This is also apparent from the data reported by Jiji and Clark [7], for which they defined a 'bubble boundary layer' as the region adjacent to the heater for which the vapor bubbles remain. A notable exception is the results of van Helden et al. [17] who report that vapor bubbles regularly lift off from an artificial cavity on the heater surface following departure.

Nucleation sites near the leading edge of the heater produced the majority of vapor bubbles, and very few sites were found downstream. Even at higher heat fluxes, the most active portion of the heater, in terms of the number of nucleation sites, was clearly the first 2–3 cm of the 30-cm long heater.

Collision and coalescence of vapor bubbles was observable at all but the lowest heat flux conditions. For example, at $G = 244$ kg m^{-2} s^{-1} and $q_w = 3.52$ kW m^{-2} (Exp. no. 2a), nucleation sites were sparse and ebullition was well ordered. As the heat flux is increased to $q_w = 6.92$ kW m^{-2} (Exp. no. 2b), the nucleation site density increases, and bubbles from neighboring sites are occasionally observed to collide and coalesce. The waiting time also decreases. Upon further increasing the heat flux to $q_w = 10.9$ kW m^{-2} (Exp. no. 2c), coalescence regularly occurs between bubbles emanating from the same nucleation site. The waiting time decreases to a point where a new bubble forms and grows at the nucleation site faster than the previous bubble can slide away, resulting in collision and coalescence of the two bubbles. At even higher heat fluxes this waiting time becomes indistinguishably short, and a bubble will at times undergo repeated collisions at the site before it is large enough to finally escape under the influence of buoyancy and/or drag.

At these higher heat fluxes, the flow near the surface becomes bubbly and chaotic, with neighboring bubbles

Table 2
Forced convective nucleation data

Exp. no.	G (kg m^{-2} s^{-1})	T_{sat} (°C)	ΔT_{sat} (°C)	ΔT_{sub} (°C)	Ja	q_w (kW m^{-2})	h (Wm^{-2} K^{-1})	$K\times10^3$ (m s^{-n})	n	d_d (mm)	No. of observ	d_L (mm)	No. of observ	t_w (ms)	No. of observ
Upflow															
1a	195	39.9	0.54	2.98	0.73	2.83	805	1.13	0.400	0.094	(98)			2.23	(92)
1b	192	39.8	2.39	2.83	3.23	4.80	920	2.46	0.463	0.165	(44)			22.2	(42)
1c	194	39.8	4.38	2.86	5.95	7.36	1017	4.07	0.500	0.207	(8)			4.67	(6)
2a	244	40.2	0.55	3.06	0.73	3.52	976	1.03	0.361	0.105	(110)			1.58	(106)
2b	258	40.2	3.15	3.27	4.28	6.92	1077	1.69	0.400	0.147	(83)			6.38	(79)
2c	255	40.0	6.34	2.78	8.56	10.9	1201	2.15	0.400	0.199	(53)			*	*
3a	315	40.3	1.32	2.52	1.74	3.63	945	1.26	0.419	0.112	(124)			2.23	(121)
3b	319	40.2	4.04	2.29	5.33	7.26	1147	1.58	0.408	0.160	(59)			1.31	(63)
3c	315	39.9	6.89	1.96	9.04	11.8	1338	2.05	0.404	0.204	(27)			*	*
Downflow†															
4a	193	40.6	0.05	4.91	0.07	1.32	267	0.82	0.401	0.131△	(4)	0.260	(4)	159.5	(2)
4b	192	40.6	4.60	4.28	6.43	4.78	538	1.23	0.374	0.157△	(77)	0.324	(40)	9.29	(76)
4c	197	40.5	6.34	4.20	8.89	7.54	715	1.89	0.443	0.187△	(31)	0.348	(20)	1.58	(6)
5a	246	40.8	2.95	4.78	4.15	3.24	418	1.29	0.413	0.134△	(81)	0.254	(65)	5.07	(61)
5b	247	40.8	5.23	4.71	7.35	4.82	485	2.22	0.458	0.167□	(32)	0.286	(45)	2.41	(22)
5c	247	40.7	7.06	4.49	9.90	7.67	664	2.55	0.484	0.148△	(59)	0.259	(56)	1.64	(14)
6a	315	41.0	3.18	5.00	4.45	3.93	469	1.00	0.384	0.150□	(20)	0.193	(34)	*	*
6b	313	41.1	5.08	4.84	7.09	5.04	495	2.05	0.495	0.112□	(73)	0.280	(32)	*	*
6c	311	41.1	6.30	4.79	8.79	6.66	583	2.59	0.500	0.132□	(50)	0.226	(37)	*	*
7	666	42.3	7.17	3.89	9.40	14.6	1319	2.91	0.488	0.123▽	(80)	0.186	(57)	1.69	(28)
Vertical pool boiling															
8	0	38.4	3.44	0.99	4.54	4.42	997	1.54	0.343	0.237	(34)	0.566	(34)	9.36	(30)

* Insufficient data due to collisions between bubbles which emanate from the same nucleation site.
† Symbols represent bubble departure and sliding direction: △ = upward; ▽ = downward; □ = transitional, as described in Section 4.2.

colliding and numerous intermittent sites participating. Based on random fluctuations in the observed bubble trajectory, the flow near the wall appears to be highly turbulent. Under these conditions bubble lift-off was observed to occur on occasion. It appeared that a turbulent eddy or a passing bubble in the bulk liquid flow would randomly sweep the surface and lift a bubble off. Further downstream the entire flow field is bubbly and highly chaotic. Because lift-off occurred infrequently except during bubbly flow, and its occurrence appears to be random, lift-off diameters were not recorded for upflow.

3.2. *Downflow*

In downflow boiling, the buoyancy force experienced by a vapor bubble is in the opposite direction of the quasi-steady drag exerted by the liquid flow. As a result, three scenarios of sliding bubbles were observed, which depend largely on the local liquid velocity. These scenarios are demonstrated in Fig. 4, where photographs of bubble ebullition are shown at three different mass fluxes, $G = 246$, 315, and 666 kg m^{-2} s^{-1} (Exp. nos. 5a, 6a, and 7). In Fig. 4(a), the bubbles rise against the oncoming flow, behaving similarly to that of upflow. The conditions under which this behavior is observed are marked with the symbol (△) in Table 2. However, bubbles do not slide far from the nucleation site before they lift off the surface into the bulk flow. Unlike in upflow, lift-off is not a result of bulk turbulence or bubble-induced turbulence, but instead is continuous and regular. This is consistent with the supposition of Zeng et al. [21] that for the downflow configuration the shear lift force should lift the bubble off the surface. As the liquid velocity is increased, the bubble slides downward in the same direction as the bulk flow. This is marked in Table 2 by the symbol (▽) and is

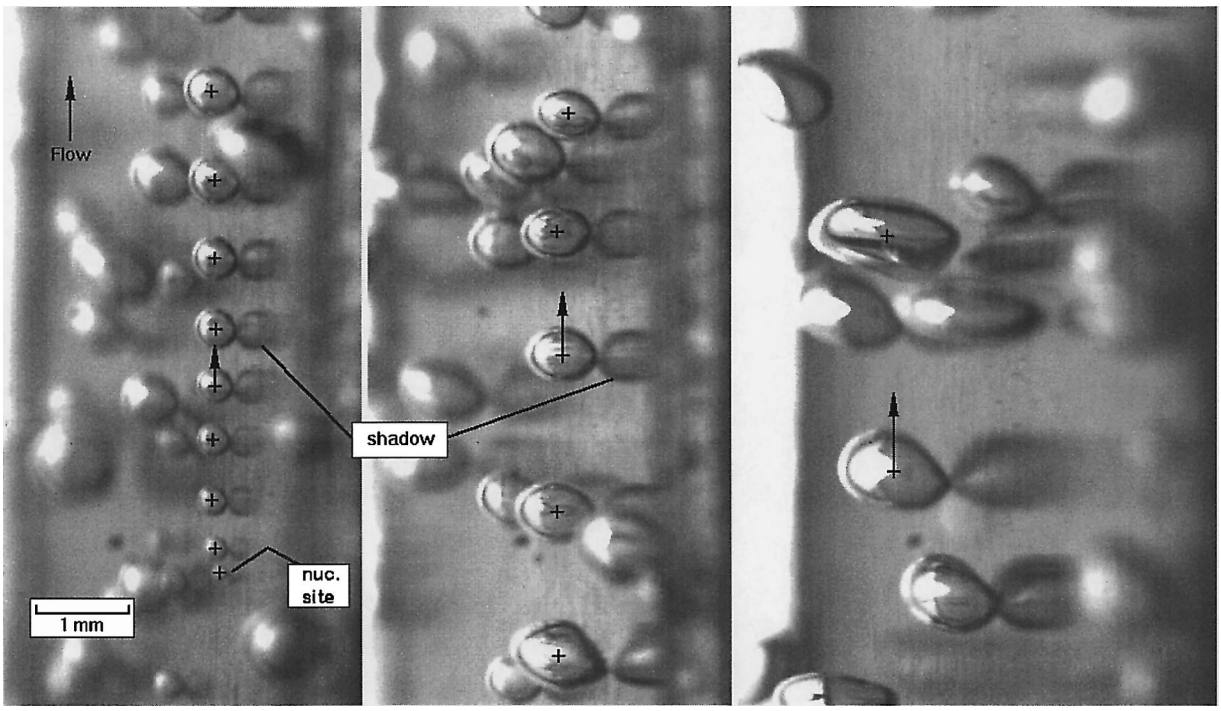

Fig. 3. Photographs of bubbles originating from a single nucleation site in upflow, $G = 258$ kg m^{-2} s^{-1}, $\Delta T_{sat} = 3.15$°C (Exp. no. 2b). (a) At the nucleation site; (b) approximately 10 mm downstream of site; (c) approximately 30 mm downstream of site.

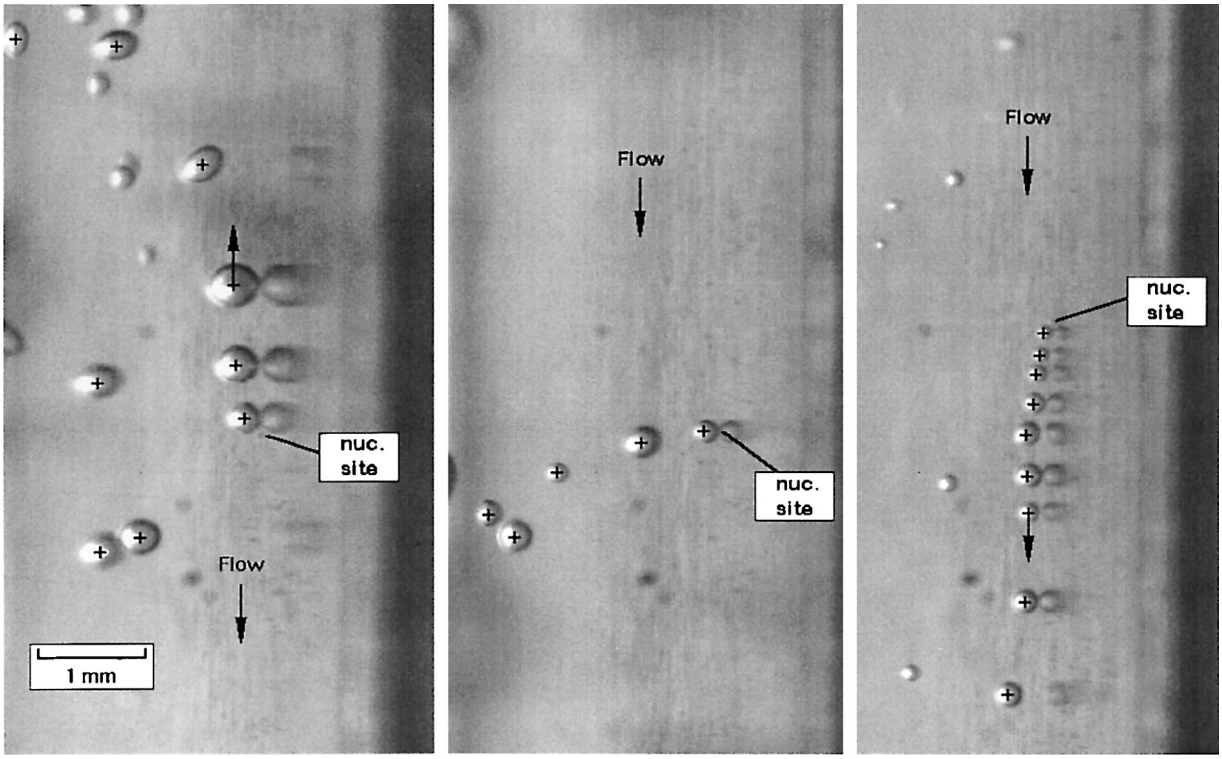

Fig. 4. Photographs of bubbles originating from a nucleation site in downflow boiling. (a) $G = 246$ kg m^{-2} s^{-1}, $\Delta T_{sat} = 2.95$°C (Exp. no. 5a); (b) $G = 315$ kg m^{-2} s^{-1}, $\Delta T_{sat} = 3.18$°C (Exp. no. 6a); (c) $G = 666$ kg m^{-2} s^{-1}, $\Delta T_{sat} = 7.34$°C (Exp. no. 7).

shown in Fig. 4(c). Lift-off occurs regularly, since the bubble still lags the surrounding flow. At elevated heat flux, bubble coalescence and eddies are observed in downflow as in upflow. Regardless of liquid velocity, the bubble sliding trajectory is much shorter in downflow compared with upflow due to lift-off.

As expected, there exists a transitional condition in downflow where bubble sliding is either upward or downward. This was observed in Exp. nos. 5b and 6a–c, where sliding took place with or against the flow with no dominant direction. These are marked in Table 2 with the symbol (□). At times a bubble would simply remain attached to the site or remain within close proximity of the site. Figure 4(b) depicts a single photograph of a stream of vapor bubbles emanating from a nucleation site in which sliding is completely absent. Under these conditions sliding does not occur. As a result, the bubble continues to grow at the nucleation site until lifted off the surface. Smaller bubbles were often observed to grow in the wake of the larger bubble and coalesce with it.

Bubble sliding is likely responsible to some extent for energy removal from the heating surface in vertical upflow. This point can be seen in Fig. 5, where values of heat transfer coefficient, defined as $h = q_w/\Delta T_{sat}$, are plotted for the upflow and downflow conditions of Table 2. From the figure, it is clear that the heat transfer coefficient is greater for upflow than for downflow at otherwise similar flow and thermal conditions. Since vapor bubbles continue to slide along the heating surface during upflow, it is reasonable to conclude that the higher heat transfer rates observed during upflow boiling as compared with downflow are due to bubble sliding. Other investigators who have found sliding bubble heat transfer to be important include Cornwell [2], Tsung-Chang and Bankoff [16], Houston and Cornwell [5], Yan and Kenning [19], and Yan et al. [20].

3.3. *Vertical pool boiling*

For the purpose of comparison, one boiling condition was examined under zero bulk flow conditions, which is listed as Exp. no. 20 in Table 2. A photograph of the ebullition process is presented in Fig. 6. As in downflow, the bubbles regularly lift off from the surface, although during sliding, bubbles actually appear detached from the heater surface. However, since there is no bulk fluid motion, the rising bubble experiences no significant velocity gradient from the surrounding fluid. Natural convection is estimated to have a negligible influence on the bubble motion. As a result, there is no shear lift of the type described by Zeng et al. [21], and therefore another force must be responsible for lift-off. The force respon-

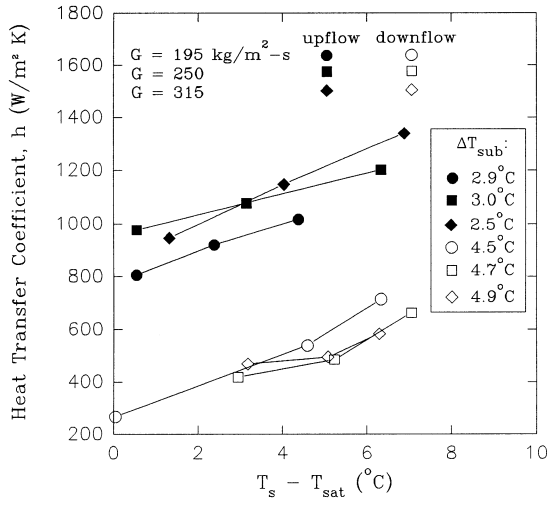

Fig. 5. Plot of heat transfer coefficient, h, vs wall superheat, $T_s - T_{sat}$, for the upflow and downflow conditions in Tables 1 and 2.

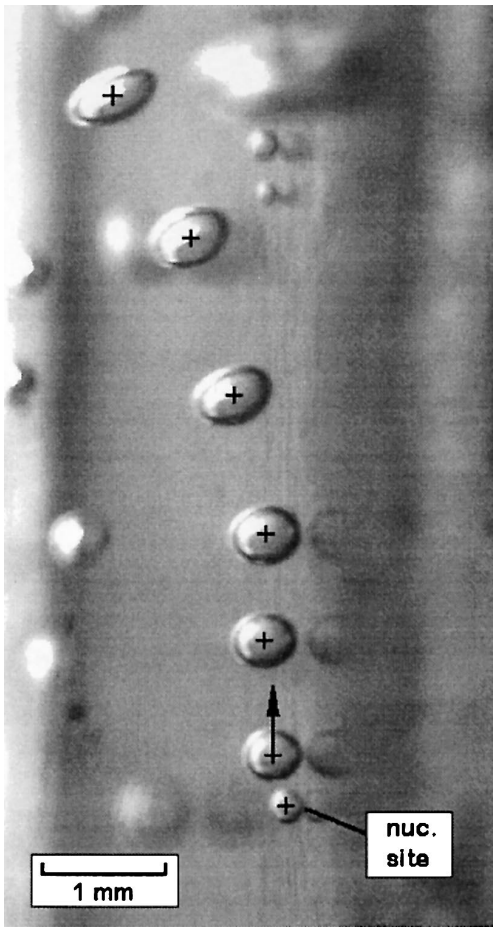

Fig. 6. Photograph of bubbles originating from the same nucleation site in vertical pool boiling, $\Delta T_{sat} = 3.44$°C (Exp. no. 8).

sible for vapor bubble lift-off during vertical pool boiling has yet to be identified and requires further investigation.

4. Bubble dynamic measurements

4.1. *Growth rate*

A typical set of experimentally measured growth curves is depicted in Fig. 7. A growth curve was obtained by measuring the diameter of an individual bubble from incipience through sliding. All the bubble growth data reported in this work lie in the diffusion-controlled regime; the inertia-controlled regime lasts for a very short period and is shorter than the time period between successive frames obtained with high-speed imaging. The experimental growth rates may be approximated by a power law curve fit,

$$d(t) = Kt^n \tag{1}$$

where $d(t)$ is the diameter of the bubble, t denotes time, K and n are empirical constants. Because of the stochastic nature of the flow and thermal variations discussed in Section 3.2., a set of 5 growth curves were measured at various points in the film set, and the constants K and n were averaged to estimate the mean growth curve at this condition. During downflow boiling, the growth showed more variation; therefore a set of 10 growth curves were obtained at each condition. The averaged growth constants for upflow and downflow are included in Table 2. The Jacob number, Ja, is included in the table for each condition.

From the table it is observed that the growth data fit a power law ranging from about $t^{1/3}$ to $t^{1/2}$. The upper limit, $t^{1/2}$, is expected, since $t^{1/2}$ is the diffusion-controlled growth limit in saturated boiling. Lower values are partly a result of energy depletion in the heater surface near the nucleation site. Recently, Mei et al. [14] developed a numerical model for vapor bubble growth in saturated pool boiling, and demonstrated that the bubble growth rate is reduced due to the resulting temperature gradients beneath the nucleation site. It seems reasonable, then, that this behavior plays a role in subcooled flow boiling as well, although the subcooling and the bulk motion of the fluid also affect the vapor bubble growth rate, as will be seen.

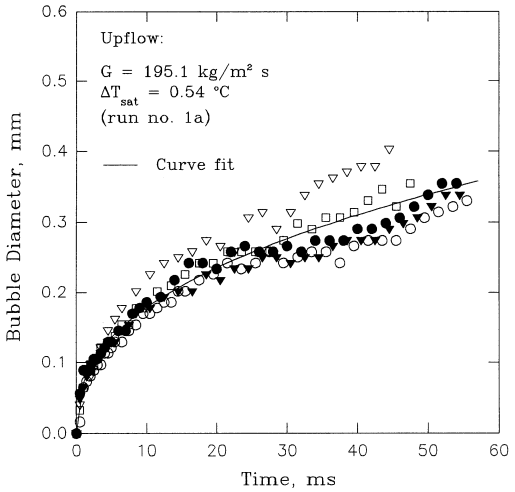

Fig. 7. Typical bubble growth measurement.

A graphical comparison of the growth curves reveals useful information about the ebullition process. Figures 8(a) and (b) depict the mean growth curves for upflow and downflow, respectively. On both graphs, the number assigned to each curve represents the experiment number listed in Table 2. The solid triangles on both sets of curves represent the departure diameter at each condition. The upflow growth curves end approximately at the point where the vapor bubbles leave the field of view, except for curves 1c, 2b, 2c, 3b, and 3c, where bubble collisions and coalescence limited the available growth data. The downflow curves end when the bubbles lift off from the heater surface, except for curve 4a, which extends beyond the limits of the plot.

Examining both graphs, several trends are clear: (1) At a given mass flux, the bubble growth increases with increasing Ja (increasing ΔT_{sat}). In fact, Kandlikar et al. [9] report a similar result for subcooled horizontal flow boiling of water, and Mei et al. [14] demonstrated the same trend analytically for pool boiling; (2) Departure from the nucleation site occurs early in the growth curves, particularly in upflow, and therefore a large portion of bubble growth occurs during the sliding phase.

The effect of varying mass flux can be seen in both figures. In upflow it appears that, at low ΔT_{sat} (or Ja), the variation of mass flux has little impact on growth, as evidenced by curves 1a, 2a, and 3a in Fig. 8(a), which represent conditions with roughly similar ΔT_{sat} (or Ja). At higher wall superheat/Jacob number, the growth curves appear to separate, although this effect is less obvious since the wall superheat/Jacob number was not held constant. What is clear, however, is that the growth at these higher wall superheats/Jacob numbers *decreases* with *increasing* G. This is evident when comparing curves 1b, 2b, and 3b, and the curves 1c, 2c, and 3c, in which the growth decreases with increasing G despite a slight increase in ΔT_{sat} (or Ja) in some cases. The same effect can be seen in Fig. 8(b) for downflow by examining the curves 4b, 5a, and 6a, and the curves 4c, 5b and 6b. Similarly, Kandlikar et al. [8, 9] also report a significant decrease in bubble growth rate as the Reynolds number is increased in horizontal subcooled flow boiling of water.

An additional observation in the downflow growth curves deserves comment. At elevated ΔT_{sat}, as is the case for conditions 4c, 5c, and 7 in Fig. 8(b), all with nearly

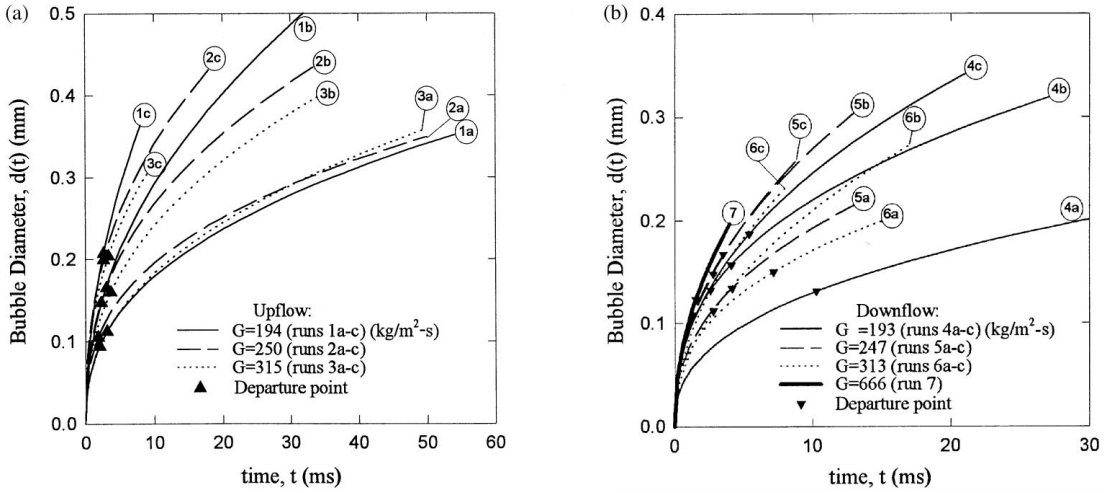

Fig. 8. Comparison of mean growth curves: (a) upflow; (b) downflow. End of upflow curves represent limits of measuring diameter, due to either end of viewfield or coalescence. End of downflow curves represent mean lift-off diameter.

the same value of wall superheat (approximately 7°C), the growth rates do not vary appreciably despite large changes in G (247–666 kg m^{-2} s^{-1}). Since n approaches 0.5, which is the maximum value for diffusion-controlled growth in saturated boiling, it can be concluded that microlayer evaporation is dominant and condensation is negligible.

4.2. *Departure and lift-off diameter*

For measuring purposes, the departure diameter, d_d, is taken to be the diameter of the bubble immediately after the first sign of displacement from the nucleation site. Similarly, the lift-off diameter, d_L, is measured immediately after the bubble detaches from the heater surface. This method was also chosen by Klausner et al. [11] in their measurement of departure and lift-off diameters. A source of uncertainty in the measurement of bubble departure diameter arises because departure occurs early in the growth curve, when the bubbles are small and the diameter is increasing rapidly. As a result, the uncertainty on the departure diameter is estimated to be within ± 0.04 mm, while the uncertainty on lift-off diameter is estimated to be ± 0.02 mm. Furthermore, bubble collisions, particularly at the nucleation site as described in Section 4.1., limit the available departure and lift-off diameter and waiting time data under some conditions. Mean values of d_d, d_L, and t_w at each experimental condition are included in Table 2. As discussed in Section 4.1, few bubbles were observed to lift off in upflow, and therefore no data for lift-off in upflow are presented.

4.2.1. *Comparison of mean departure and lift-off diameter data*

Figure 9 compares the mean values of departure diameter, d_d, at various values of mean liquid velocity as a function of wall superheat, ΔT_{sat}, for (a) upflow and (b) downflow. Also included in both plots is the mean departure diameter under vertical pool boiling, obtained in the same experimental facility under zero flow conditions. In upflow it is seen that the departure diameter clearly increases with increasing wall superheat; this is due to the increased bubble growth at higher wall superheat. The expanding vapor bubble generates a reaction force, referred to as the growth force, in the surrounding liquid which resists bubble motion away from the heater wall. The departure diameter appears to decrease with increasing mean liquid velocity in upflow, although beyond $G \approx 250$ kg m^{-2} s^{-1} there is little change in d_d with G.

In downflow, interpretation of the departure diameter data is complicated by the fact that bubbles depart either upward or downward. Under conditions where the bubbles slide upward against the flow, the departure diameter increases with increasing ΔT_{sat}, similar to upflow, although the values of d_d tend to be lower in downflow. On the other hand, at all other conditions, trends in the d_d data are less clear. Despite the differences in the data it appears that, as in upflow, the departure diameter generally decreases with increasing mean liquid velocity.

Figure 10 depicts mean lift-off diameters obtained for downflow and vertical pool boiling at various mean liquid velocities. The lift-off diameter data follow similar behavior as departure diameter: in general d_L increases slightly with ΔT_{sat} and decreases with G. Both of these trends are expected. An increase in ΔT_{sat} results in an increased growth rate, and therefore a larger growth force exists which resists lift-off. Conversely, an increase in mass flux results in a higher shear lift force which promotes lift-off. Again, the variation of d_L with ΔT_{sat} is not discernable at $G \approx 250$ and 315 kg m^{-2} s^{-1}. It is evident, however, that the bubble lift-off diameter tends to

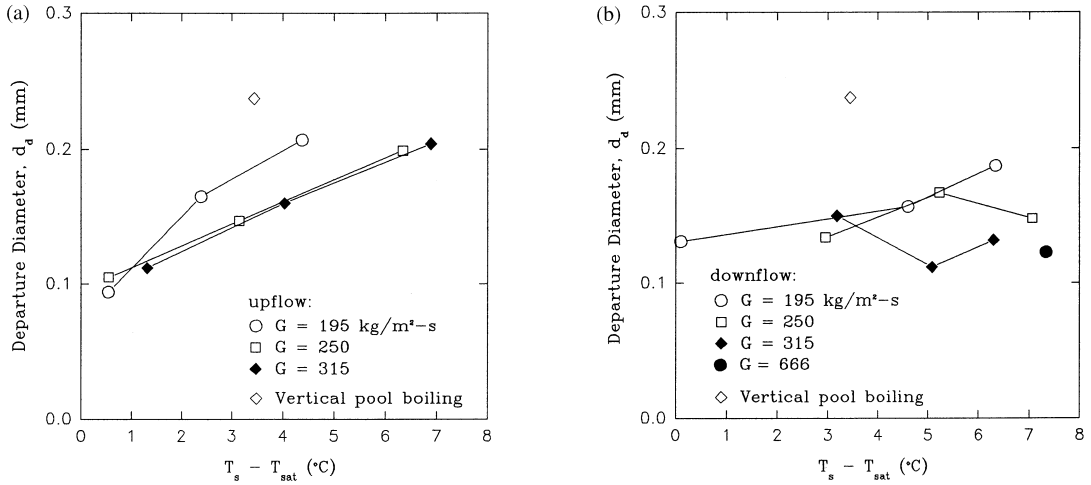

Fig. 9. Comparison of measured mean departure diameters for (a) upflow and (b) downflow forced convection boiling. Diamond (◇) represents vertical pool boiling data point.

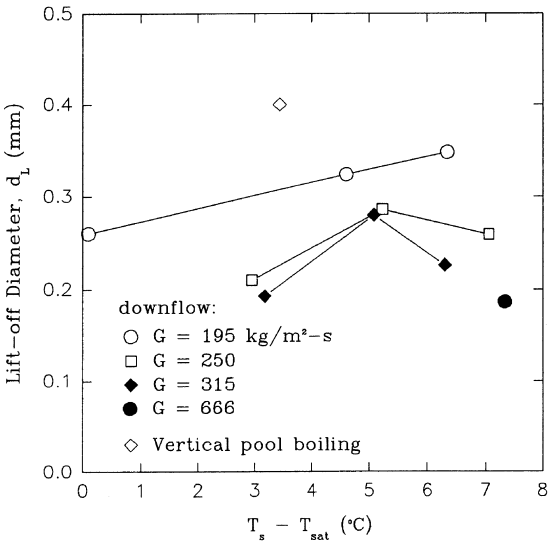

Fig. 10. Comparison of measured mean lift-off diameters in downflow forced convection and vertical pool boiling.

decrease with increasing G, which may be due to an increasing shear lift force.

4.2.2. *Comparison of departure and lift-off diameter probability functions*

To gain additional insight into the stochastic nature of the bubble removal process, probability functions of departure and lift-off diameter were obtained from selected experimental data. Strictly speaking, the experimental data samples are not large enough (approximately 50 realizations) to construct probability functions with sufficient statistical accuracy. The functions are instead reported to demonstrate qualitative features of departure and lift-off behavior.

Figure 11(a)–(c) depicts probability functions of departure diameter obtained from the experimental data for 3 values of mean liquid velocity for upflow. Despite the small sample sizes, the distributions resemble a Gaussian distribution although they are slightly skewed. For upflow, the standard deviation of each distribution is consistently close to 1/10th the mean value, and therefore the standard deviation increases with mean departure diameter for increasing wall superheat. This result is similar to that reported by Klausner et al. [11], who suggested that the origin of the stochastic behavior is the turbulent fluctuations of the liquid velocity, as well as spatial and temporal fluctuations of wall superheat which affect the bubble growth rate. Recently, Klausner et al. [10] developed a model which predicts the stochastic variations of departure and lift-off diameter from estimates of the distribution of bulk liquid velocity and wall superheat. However, their model requires a method for predicting vapor bubble growth rate as a function of wall superheat, which at present is not available for subcooled vertical flow boiling. Therefore no attempt has been made to apply their model to the present data.

Figure 12(a)–(b) depict probability functions of departure diameter for downflow. Again it appears that both the mean departure diameter and the standard deviation typically increase with increasing wall superheat. However, due to the varying direction of bubble departure the relative value of the standard deviation is less consistent than for upflow. Figure 13(a)–(b) depict probability functions of lift-off diameter for the same downflow conditions. For lift-off diameters, trends in the mean or standard deviation are less clear, although the standard deviation appears to decrease with increasing wall superheat.

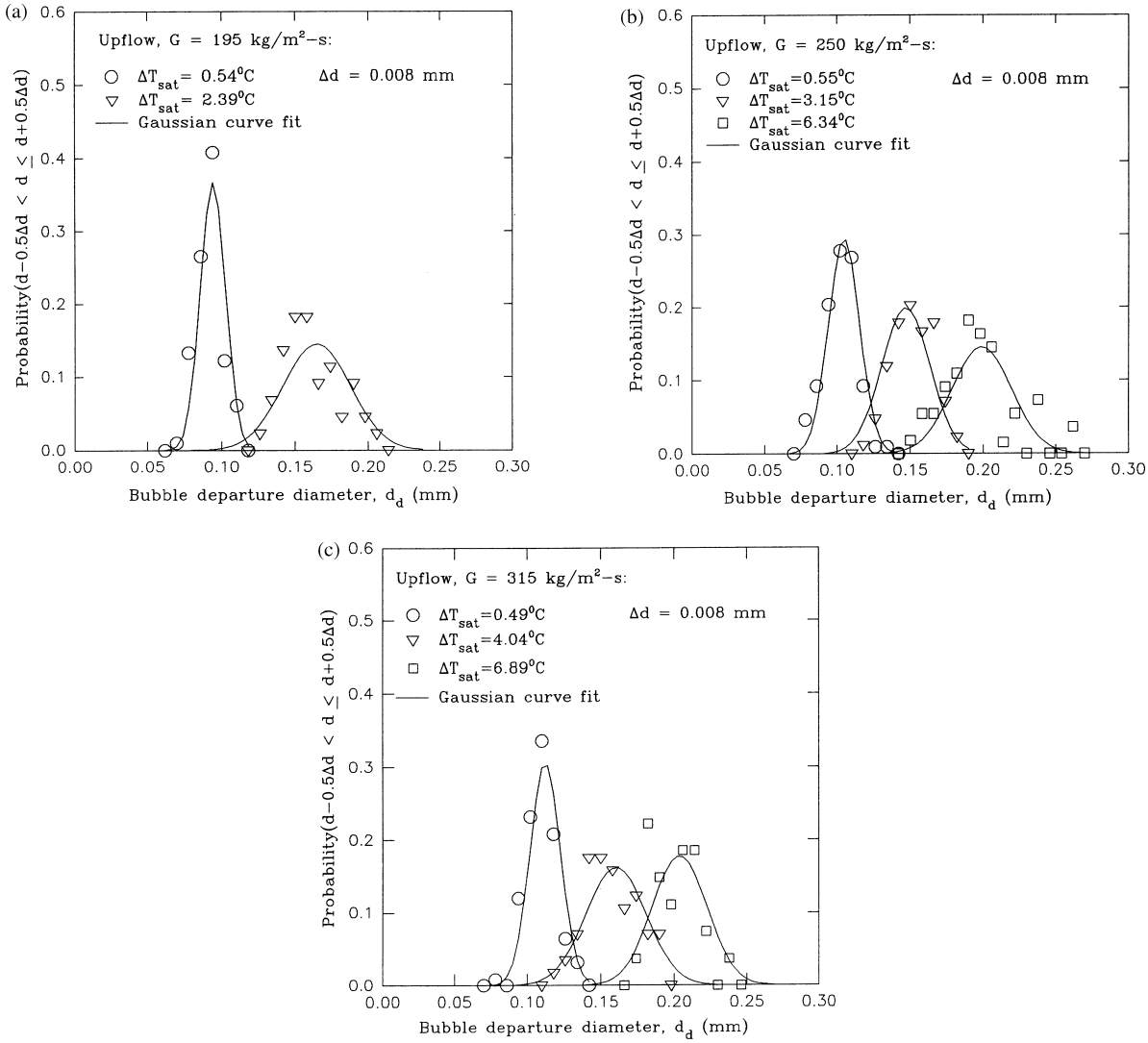

Fig. 11. Departure diameter probability functions at various mass fluxes and wall superheats in upflow forced convection boiling.

4.3. *Waiting time*

Waiting time, t_w, is defined as the time between bubble departure and the incipience of the next bubble at the same nucleation site. Mean waiting times are included in Table 2. Examining the tabular data, it appears that t_w tends to decrease with increasing heat flux. This is expected, since at higher heat flux the local temperature field beneath a nucleation site will recover more quickly. At higher heat flux, the waiting times are so short that collisions occur regularly between bubbles emanating from the same site, as described in Section 4.1, and the waiting times under these conditions become too short to resolve within the temporal resolution of the film. Conditions under which waiting times could not be resolved are marked in Table 2 by asterisks (*).

From the film data it is possible to demonstrate a relationship between waiting time and departure diameter. Figure 14 illustrates a sequential plot of departure diameters and associated waiting times obtained from one vertical upflow boiling condition. From this plot it is evident that an increase in departure diameter is followed by a proportional increase in waiting time. This direct proportionality can be explained in terms of energy depletion from the heater surface, as demonstrated by Mei et al. [14]. A larger departure diameter implies that more energy has been depleted from the solid heater beneath the nucleation site, and as a result the local temperature field in the heater takes longer to recover. It is reasonable to conclude, then, that stochastic variations in the departure diameter, as shown in Figs 11–13, are related to variations in the temperature of the heater

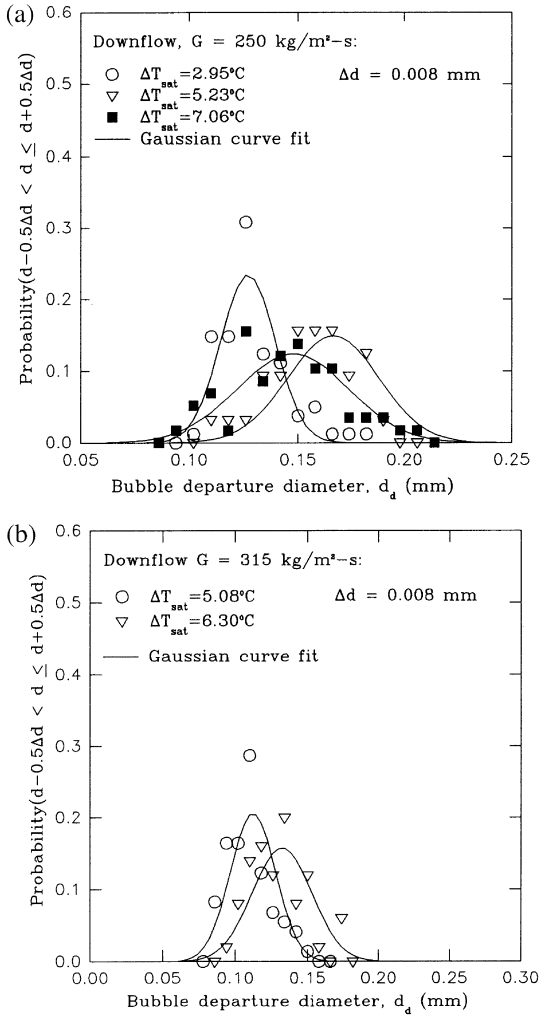

Fig. 12. Departure diameter probability density functions at various mass fluxes and wall superheats in downflow boiling.

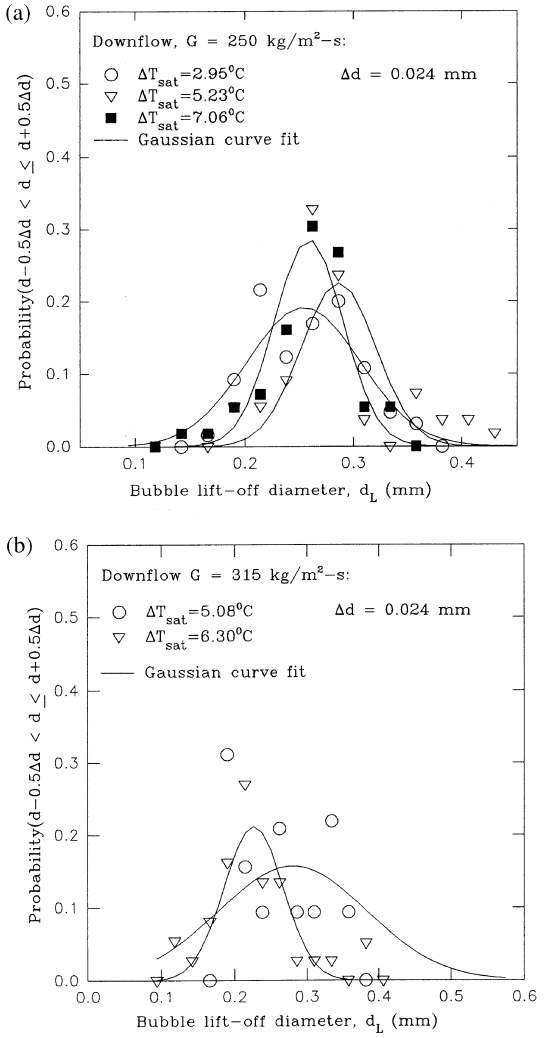

Fig. 13. Lift-off diameter probability density functions at various mass fluxes and wall superheats in downflow.

surface. This is indeed the result suggested by Klausner et al. [10].

5. Conclusions

Visual observations of ebullition in upflow and downflow boiling reveal several important features:

(1) A relatively small portion of bubble growth occurs while the bubble is attached to the nucleation site; most growth occurs during the sliding process, particularly in upflow.
(2) Vapor bubble lift-off is not generally observed in upflow, except occasionally due to random velocity fluctuations. In contrast, lift-off regularly occurs in downflow.
(3) Substantial evidence reveals that vapor bubble sliding enhances the energy transfer at the heating surface. First, the heat transfer coefficient is significantly higher for upflow than downflow at otherwise identical flow and thermal conditions. Second, in upflow boiling the most active nucleation sites were found close to the leading edge of the heater, suggesting that nucleation is being suppressed downstream due to enhanced energy transport.

Vapor bubble growth, departure diameter, and lift-off diameter data have been obtained for upflow and downflow boiling for $G = 192$–666 kg m^{-2} s^{-1} and $q_w = 1.3$–14.6 kW m^{-2}, at slightly subcooled conditions ($\Delta T_{sub} = 1.0$–5.0°C) during which isolated nucleation sites are active. The data reveal a number of interesting

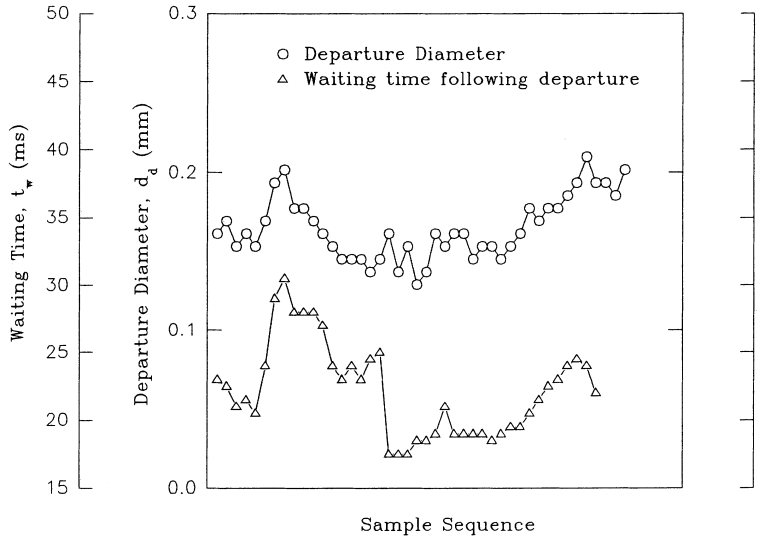

Fig. 14. Sequence of measured departure diameters and associated waiting times for upflow boiling from the same nucleation site, $G = 192$ kg m^{-2} s^{-1}, $\Delta T_{sat} = 2.39$°C (Exp. no. 1b). Sequence spans approximately 800 ms.

features associated with the vapor bubble dynamics during vertical flow boiling:

(1) Bubble growth increases with Jacob number (increasing ΔT_{sat}) under otherwise identical conditions in upflow or downflow. Conversely, bubble growth generally decreases with increasing mass flux, which may be a result of operating at slightly subcooled conditions, during which the increased mass flux provides increased condensation at the top of the bubble.
(2) Bubble departure diameter increases with Jacob number (increasing ΔT_{sat}) and decrees with increasing mass flux in both upflow and downflow.
(3) Lift-off diameters in downflow were observed to decrease with increasing mass flux, and show a possible increase with increasing Jacob number (increasing ΔT_{sat}).
(4) Waiting times were observed to decrease with increasing heat flux, which is related to energy depletion at the heater surface. Furthermore, waiting time and departure diameter are observed to be directly correlated.

Acknowledgements

This work was performed while the lead author was supported as a Florida Space Grant Fellow. The authors also wish to thank 3M Corporation for donating the perfluorocarbon fluids used in this work, and Dr Dan Hanes of the UF Department of Coastal and Oceanographic Engineering for the use of their digital high-speed imaging facility. The financial support provided by the Exxon Education Foundation under Grant No. 04/1995 is greatly appreciated.

References

[1] Cooper MG, Mori K, Stone, CR. Behavior of vapour bubbles growing at a wall with forced flow. Int J Heat Mass Transfer 1983;26(10):1489–1507.
[2] Cornwell K. The influence of bubbly flow on boiling from a tube in a bundle. Int J Heat Mass Transfer 1990;33(12):2579–84.
[3] Frost W, Kippenhan CJ. Bubble growth and heat transfer mechanisms in the forced convection boiling of water containing a surface active agent. Int J Heat Mass Transfer 1967;10:931–49.
[4] Gunther FC. Photographic study of surface-boiling heat transfer to water with forced convection. Trans ASME 1951;73:115–24.
[5] Houston SD, Cornwell K. Heat transfer to sliding bubbles on a tube under evaporating and non-evaporating conditions. Int J Heat Mass Transfer 1995;39(1):211–4.
[6] Hsu YY, Graham RW. A visual study of two-phase flow in a vertical tube with heat addition. NASA Technical Note D-1564, 1963.
[7] Jiji LM, Clark JA. Bubble boundary layer and temperature profiles for forced convection boiling in channel flow. Journal of Heat Transfer 1964;86:50–8.
[8] Kandlikar SG, Cartwright MD, Mizo VR. A photographic study on nucleation characteristics of cavities in flow boiling. In: Chen JC, editor. Convective flow boiling. Washington D.C.: Taylor and Francis, 1996. pp. 73–8.
[9] Kandlikar SG, Mizo VR, Cartwright MD. Investigation of bubble departure mechanism in subcooled flow boiling of water using high-speed photography. In: Chen JC, editor.

Convective flow boiling. Washington D.C.: Taylor and Francis, 1996. pp. 161–6.
[10] Klausner JF, Mei R, Zeng LZ. Predicting stochastic features of vapor bubble detachment in flow boiling. Int J Heat Mass Transfer 1997;40(15):3547–52.
[11] Klausner JF, Mei R, Bernhard DM, Zeng LZ. Vapor bubble departure in forced convection boiling. Int J Heat Mass Transfer 1993;36:651–62.
[12] Koumoutsos N, Moissis R, Spyridonos A. A study of bubble departure in forced-convection boiling. Journal of Heat Transfer 1968;90:223–30.
[13] Lyons SL. A direct numerical simulation of turbulent channel flow with passive heat transfer. Ph.D. Thesis, University of Illinois at Urbana-Champaign, 1989.
[14] Mei R, Chen W, Klausner JF. Vapor bubble growth in heterogeneous boiling—II. Growth rate and thermal fields. Int J Heat Mass Transfer 1995;38(5):921–34.
[15] Thorncroft GE. Heat transfer and vapor bubble dynamics in forced convection boiling. Ph.D. Thesis, University of Florida, Gainesville, Florida, 1997.
[16] Tsung-Chang G, Bankoff SG. On the mechanism of forced-convection subcooled nucleate boiling. J Heat Transfer 1990;112:213–8.
[17] van Helden WGJ, van der Geld CWM, Boot PGM. Forces on bubbles growing and detaching in flow along a vertical wall. Int J Heat Mass Transfer 1995;38(11):2075–88.
[18] van der Geld CW, van Helden WG, Boot PG. On the effect of the temperature boundary condition on single bubble detachment in flow boiling. In: Chen JC, editor. Convective flow boiling. Washington D.C.: Taylor and Francis, 1996. pp. 149–54.
[19] Yan Y, Kenning DBR. Flow boiling in bubbly flow. In: Chen JC, editor. Convective flow boiling. Washington D.C.: Taylor and Francis, 1996. pp. 293–8.
[20] Yan Y, Kenning DBR, Cornwell K. Sliding and sticking vapour bubbles under inclined plane and curved surfaces. Eurotherm 48. Pool Boiling Conf., Paderborn. 1996.
[21] Zeng LZ, Klausner JF, Mei R. A unified model for the prediction of bubble detachment diameters in boiling systems—I. Flow boiling. Int J Heat Mass Transfer 1993;36(9):2271–9.